Inorg. Chem. **2009**, *48*, 953−963

Inorganic Chemistry
Article

The Hydrothermal and Structural Chemistry of Oxovanadium−Arylphosphonate Networks and Frameworks

Wayne Ouellette,[†] Guangbin Wang,[‡] Hongxue Liu,[§] Gordon T. Yee,[‡] Charles J. O'Connor,[§] and Jon Zubieta*,[†]

Departments of Chemistry, Syracuse University, Syracuse, New York 13244, Virginia Polytechnic Institute and State University, Blacksburg, Virginia 24061, and University of New Orleans, New Orleans, Louisiana 70148

Received July 31, 2008

The hydrothermal reactions of NH_4VO_3 with the aromatic phosphonate ligands 1,4-, 1,3-, and 1,2-phenylenediphosphonic acids (H_4L1, H_4L3, H_4L4, respectively); biphenyl-4,4′-diyldiphosphonic acid (H_4L2); and 1,3,5-tris(phenyl)-4,4′-triphosphonic acid (H_6L5) yielded materials of the V_xO_y/organophosphonate family $[VO(H_2L1)]$ (**1**), $[VO(H_2L2)]$ (**2**), $[V_2O_2(H_2O)_2(L3)]\cdot 1.5H_2O$ (**3**$\cdot 1.5H_2O$), $[V_2O_2(H_2O)_2(L4)]\cdot 2H_2O$ (**4**$\cdot 2H_2O$), and $[V_3O_3(OH)(H_3L5)_2]\cdot 7.5H_2O$ (**6**$\cdot 7.5H_2O$). The reactions were carried out in the presence of HF, and in one case, fluoride was incorporated to provide $[V_2F(OH)(H_2O)_3(L4)]\cdot 2.25H_2O$ (**5**$\cdot 2.25H_2O$). The materials exhibit diverse structural chemistry, including the prototypical buttressed layer architecture for **1** and **2**, a complex three-dimensional structure for **3**, and unique two-dimensional structures for **4**, **5**, and **6**. The structures of this oxovanadium−arylphosphonate family are quite distinct from those previously described for the V_xO_y/alkyldiphosphonate series.

Introduction

Metal organophosphonates are prototypical organic−inorganic composite materials, which can exhibit a range of structures including molecular clusters, chains, layers, and three-dimensional frameworks.[1] This structural versatility is reflected in applications to areas as diverse as catalysis, proton conductivity, ion exchange, intercalation chemistry, and photochemistry.[2−7]

* Author to whom correspondence should be addressed. Telfax, international code: +(315) 443-4070. E-mail: jazubiet@syr.edu.
† Syracuse University.
‡ Virginia Polytechnic Institute.
§ University of New Orleans.

(1) The chemistry of metal organophosphonates has witnessed remarkable growth in the past decade. A number of useful reviews are available: (a) Vioux, A.; LeBideau, J.; Mutin, P. H.; Leclercq, D. *Top Curr. Chem.* **2004**, *232*, 145. (b) Clearfield, A. *Curr. Opin. Solid State Mater. Sci.* **2003**, *6*, 495. (c) Clearfield, A. *Prof. Inorg. Chem.* **1998**, *47*, 371. (d) Alberti, G. In *Comprehensive Supramolecular Chemistry*; Atwood, J. L., Davis, J. E. D., Vogel, F., Eds.; Pergamon Press: New York, 1996; Vol. *9*, p 152. (e) Clearfield, A. In *Comprehensive Supramolecular Chemistry*; Atwood, J. L., Davis, J. E. D., Vogel, F., Eds.; Pergamon Press: New York, 1996; Vol. *9*, p 107. (f) Clearfield, A. *Chem. Mater.* **1998**, *10*, 2801. (g) Vermeulen, L. A. *Prog. Inorg. Chem.* **1997**, *44*, 143.
(2) (a) Clearfield, A. *Design of New Materials*; Cocke, D. L., Clearfield, A.; Eds.; Plenum: New York, 1986; p 121. (b) Clearfield, A. *Solvent Extr. Ion Exch.* **2000**, *18*, 655. (c) Byrd, H.; Clearfield, A.; Poojay, D. M.; Reis, K. P.; Thompson, M. E. *Chem. Mater.* **1996**, *8*, 2239.
(3) Yiing, S.-M.; Mao, J.-G. *Cryst. Growth Des.* **2006**, *6*, 964.
(4) Maeda, K. *Microporous Mosoporous Mater.* **2004**, *73*, 47, and references therein.
(5) Cheethan, A. K.; Férey, G.; Loiseau, T. *Angew. Chem., Int. Ed.* **1999**, *38*, 3269.
(6) Stern, E.; Clearfield, A.; Subramamian, M. A. *Solid State Ionics* **1996**, *83*, 113.
(7) Konar, S.; Zon, J.; Prosvirin, A. V.; Dunbar, K. R.; Clearfield, A. *Inorg. Chem.* **2007**, *46*, 5229, and references therein.
(8) Riou, D.; Serre, C.; Provost, J.; Férey, G. *J. Solid State Chem.* **2000**, *155*, 238.
(9) Riou, D.; Baltazar, P.; Ferey, G. *Solid State Sci.* **2000**, *2*, 127.
(10) Riou-Cavellec, M.; Sanselme, M.; Férey, G. *J. Mater. Chem.* **2000**, *10*, 745.
(11) Ouellette, W.; Koo, B.-K.; Burkholder, E.; Golub, V.; O'Connor, C. J.; Zubieta, J. *Dalton Trans.* **2004**, 1527.
(12) Harrison, W. T. A.; Dussack, L. L.; Jacobson, A. J. *Inorg. Chem.* **1996**, *35*, 1461.
(13) Khan, M. I.; Lee, Y.-S.; O'Connor, C. J.; Haushalter, R. S.; Zubieta, J. *Inorg. Chem.* **1994**, *33*, 3855.
(14) Khan, M. I.; Lee, Y.-S.; O'Connor, C. J.; Haushalter, R. S.; Zubieta, J. *Chem. Mater.* **1994**, *6*, 4525.
(15) Khan, M. I.; Lee, Y.-S.; O'Connor, C. J.; Haushalter, R. S.; Zubieta, J. *Chem. Mater.* **1994**, *6*, 721.
(16) Ninclaus, C.; Serre, C.; Riou, D.; Férey, G. C.R. *Acad. Sci., Ser. IIc: Chim.* **1998**, *1*, 551.
(17) Riou, D.; Serre, C.; Férey, G. *J. Solid State Chem.* **1998**, *141*, 89.
(18) Riou, D.; Roubeau, O.; Férey, G. *Microporous Mesoporous Mater.* **1998**, *23*, 23.
(19) Riou, D.; Férey, G. *J. Mater. Chem.* **1998**, *8*, 2733.
(20) Yucesan, G.; Golub, V.; O'Connor, C. J.; Zubieta, J. *Dalton Trans.* **2005**, 2241.
(21) Yucesan, G.; Golub, V.; O'Connor, C. J.; Zubieta, J. *Solid State Sci.* **2005**, *7*, 133.

10.1021/ic801450m CCC: $40.75
Published on Web 12/23/2008

Scheme 1

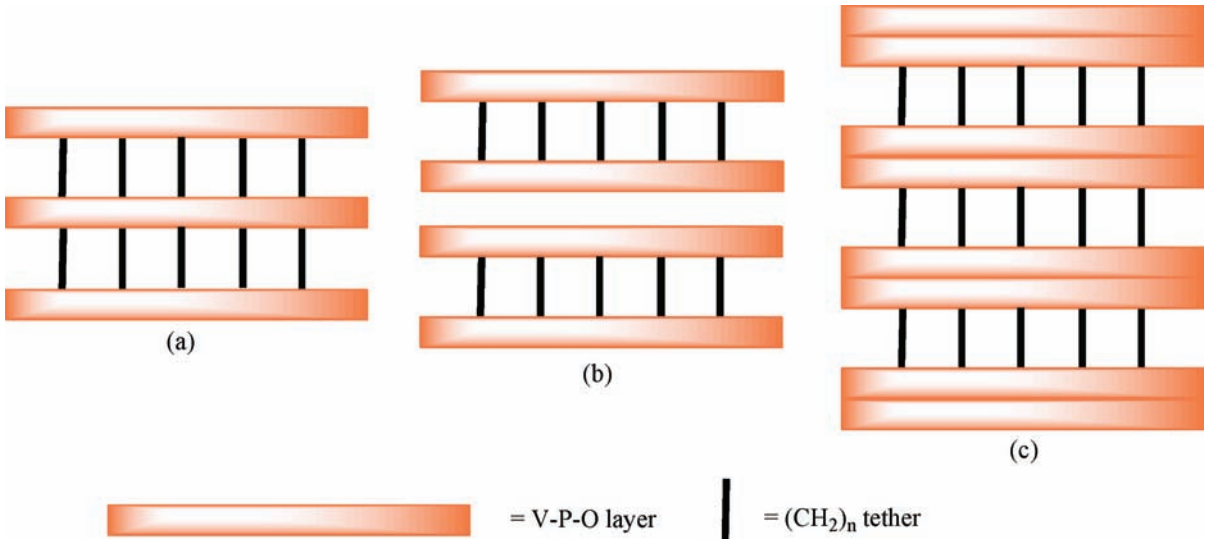

An important subclass of these materials is the oxovanadium organophosphonates,[8−24] a structurally diverse family of materials characterized by thermal stability of the V−P−O substructure, readily modified organic substituents, and distinct hydrophobic and hydrophilic domains.[25−34] A significant characteristic of the oxovanadium organophosphonate materials is the generation of well-defined internal void spaces,[35,36] which endow the materials with properties relevant to intercalation, gas storage, or electrooptical applications.[37−39] Of particular interest in this regard are the oxovanadium diphosphonate phases, materials constructed of V−P−O layers buttressed by the organic linkers of the $\{H_xO_3P\text{-tether-}PO_3H_y\}^{n-}$ ligand. Despite this recurrent theme, the detailed structural chemistry may be exceedingly complex, reflecting structural determinants such as the tether length of the diphosphonate ligand, the introduction of organic or metal−organic complex cations, and the incorporation of fluoride anions into the inorganic substructure.[40] The consequences of variations in tether lengths are illustrated in the family of materials incorporating α,ω-alkyldiphosphonate buttresses $[V_xO_y\{O_3P(CH_2)_nPO_3\}_z]$, shown in Scheme 1.[41] Thus, for $n = 2-5$, the prototypical buttressed layer structure (a) is observed. However, upon expansion of the tether length to $n = 6-8$, a two-dimensional structure arises with the organic chains sandwiched between V−P−O layers. Further expansion of the tether to $n = 9$ or 10 results in three-dimensional structures, characterized by V−P−O double layers and organic buttresses.

In an attempt to explore further the structural consequences of tether length and identity, the chemistry of vanadium oxides with aromatic di- and triphosphonates was explored. In contrast to the alkyldiphosphonates, the aromatic derivatives possess a rigid backbone. Furthermore, the geometric disposition of the $\{O_3P-\}$ groups may be readily manipulated by moving the substitution site about the ring, as shown in Scheme 2. Additional functionality is also readily introduced. In this study, we have investigated the hydrothermal chemistry of vanadium oxides with the organophosphonate ligands 1,4-, 1,3-, and 1,2-phenyldiphosphonic acid; biphenyl-4,4′-diyldiphosphonic acid; and 1,3,5-triphosphonic acid (H_4L1, H_4L3, H_4L4, H_4L2 and H_6L5, respectively), of Scheme 2. The structures of $[VO(H_2L1)]$ (**1**) and $[VO(H_2L2)]$ (**2**) are grossly similar to the prototypical buttressed layer structure previously reported for the aliphatic series $[V_2O_2(H_2O)\{O_3P(CH_2)_nPO_3\}]$ ($n = 2-5$). In contrast, the structure of $[V_2O_2(H_2O)_2(L3)]\cdot 1.5H_2O$ (**3**$\cdot 1.5H_2O$) exhibits layers linked through $\{VO_5\}$ tethers, while $[V_2O_2(H_2O)_2(L4)]\cdot 2H_2O$ (**4**$\cdot 2H_2O$) is two-dimensional. Fluoride incor-

(22) Yucesan, G.; Ouellette, W.; Golub, V.; O'Connor, C. J.; Zubieta, J. *Solid State Sci.* **2005**, *7*, 445.
(23) Yucesan, G.; Yu, M. H.; Ouellette, W.; O'Connor, C. J.; Zubieta, J. *Cryst. Eng. Comm.* **2005**, *7*, 480.
(24) Yucesan, G.; Yu, M.-H.; O'Connor, C. J.; Zubieta, J. *Cryst Eng Comm* **2005**, *7*, 711.
(25) Finn, R. C.; Zubieta, J.; Haushalter, R. C. *Prog. Inorg. Chem.* **2003**, *51*, 451.
(26) Khan, M. I.; Zubieta, J. *Prog. Inorg. Chem.* **1995**, *43*, 1.
(27) Soghomonian, V.; Chen, Q.; Haushalter, R. C.; Zubieta, J. *Angew. Chem., Int. Ed. Engl.* **1995**, *34*, 223.
(28) Soghomonian, V.; Diaz, R.; Haushalter, R. C.; O'Connor, C. J.; Zubieta, J. *Inorg. Chem.* **1995**, *34*, 4460.
(29) Soghomonian, V.; Haushalter, R. C.; Zubieta, J. *Chem. Mater.* **1995**, *7*, 1648.
(30) Bonavia, G.; Haushalter, R. C.; O'Connor, C. J.; Zubieta, J. *Inorg. Chem.* **1996**, *35*, 5603.
(31) Bonavia, G. H.; Haushalter, R. C.; Lu, S.; O'Connor, C. J; Zubieta, J. *J. Solid State Chem.* **1997**, *132*, 144.
(32) Ouellette, W.; Golub, V.; O'Connor, C. J.; Zubieta, J. *J. Solid State Chem.* **2007**, *180*, 2500.
(33) Ouellette, W.; Golub, V.; O'Connor, C. J.; Zubieta, J. *Dalton Trans.* **2005**, 291.
(34) Ouellette, W.; Koo, B.-K.; Burkholder, E.; Golub, V.; O'Connor, C. J.; Zubieta, J. *Dalton Trans.* **2004**, 1527.
(35) Johnson, J. W.; Jacobson, A. J.; Butler, W. M.; Rosenthal, S. E.; Brody, J. F.; Lewandowski, J. T. *J. Am. Chem. Soc.* **1989**, *111*, 381.
(36) Huan, G.; Jacobson, A. J.; Johnson, J. W.; Corcoran, E. W. *Chem. Mater.* **1990**, *2*, 91.
(37) Zhu, J.; Bu, X.; Feng, P.; Stucky, G. D. *J. Am. Chem. Soc.* **2000**, *122*, 11563.
(38) Barton, T. J.; Bull, C. M.; Klemperer, W. G.; Loy, D. A.; McEnaney, B.; Misino, M.; Monson, P. A.; Pey, G.; Scherer, G. W.; Vartuli, J. C.; Yaghi, O. M. *Chem. Mater.* **1999**, *11*, 2633.
(39) Cheethan, A. K.; Férey, G.; Loiseau, T. *Angew. Chem., Int. Ed.* **1999**, *38*, 3268.
(40) Ouellette, W.; Zubieta, J. *ACS Symp. Series* **2007**, *974* (Vanadium), 392.
(41) Ouellette, W.; Yu, M. H.; O'Connor, C.J.; Zubieta, J. *Inorg. Chem.* **2006**, *45*, 3224.

Scheme 2

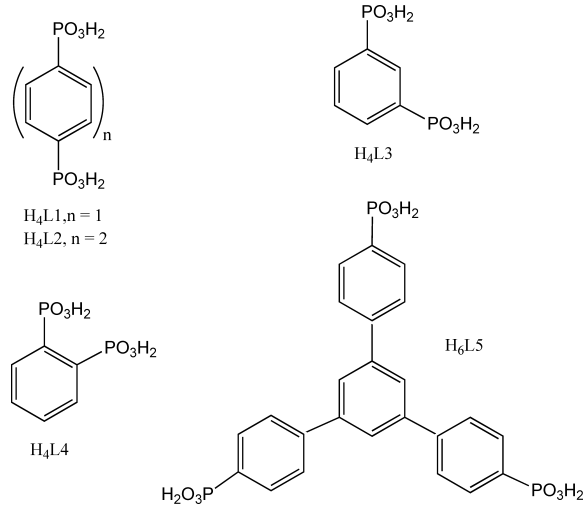

poration[42] in $[V_2F(OH)(H_2O)_3(L4)]\cdot 2.25H_2O$ (**5**·2.25 H_2O) also produces a two-dimensional phase. Incorporation of the organotriphosphonate ligand results in an unusual two-dimensional phase $[V_3O_3(OH)\{C_6H_3(C_6H_4PO_3H)_3\}]\cdot 7H_2O$/$[V_3O_3(OH)(H_3L5)]\cdot 7H_2O$ or **6**·$7H_2O$, with a trinuclear mixed valence V(V)/2×V(IV) building block.

Experimental Section

General Considerations. All chemicals were used as obtained without further purification: ammonium metavanadate, 1,2-bis-(dimethoxyphosphoryl)benzene, and hydrofluoric acid (48 to 51%) were purchased from Aldrich. The phosphonate ligands 1,3-phenylenediphosphonic acid, 1,4-phenylenediphosphonic acid, biphenyl-4,4′-diyldiphosphonic acid, and 1,3,5-tris(phenyl)-4′-triphosphonic acid benzene were prepared according to literature methods.[43] All syntheses of organic/inorganic composites were carried out in 23 mL poly(tetrafluoroethylene)-lined stainless steel containers under autogenous pressure. The reactants were stirred briefly and initial pH measured before heating. Water was distilled above 3.0 M Ω in-house using a Barnstead Model 525 Biopure Distilled Water Center. The reactions' initial and final pH were measured using Hydrion pH sticks. Elemental analyses were performed by QTI, Whitehouse, New Jersey. Sample purities were confirmed by powder XRD (Supporting Information, Tables S7−S12).

Synthesis of $[VO(H_2L1)]$ (1). A solution of NH_4VO_3 (0.182 g, 1.56 mmol), 1,4-phenylenediphosphonic acid (0.113 g, 0.720 mmol), H_2O (10.00 g, 556 mmol), and HF (0.500 mL, 14.49 mmol) at a molar ratio of 2.16:1.00:772:20.13 was stirred briefly before heating to 200 °C for 48 h (initial and final pH of 1.0 and 1.5, respectively). Green plates of **1**, suitable for X-ray diffraction, were isolated in 70% yield. IR (KBr pellet, cm^{-1}): 3515(w), 3227(b), 1630(m), 1410(m), 1178(s), 1065(s), 1025(m), 939(s), 786(m). Anal. calcd for $C_6H_6O_7P_2V$: C, 23.8; H, 1.99. Found: C, 24.2; H, 1.85.

Synthesis of $[VO(H_2L2)]$ (2). A solution of NH_4VO_3 (0.099 g, 0.846 mmol), biphenyl-4,4′-diyldiphosphonic acid (0.134 g, 0.575 mmol), H_2O (10.00 g, 556 mmol), and HF (0.200 mL, 5.80 mmol) at a molar ratio of 1.47:1.00:967:10.09 was stirred briefly before heating to 200 °C for 48 h (initial and final pH of 1.5 and 1.0, respectively). Blue plates of **2** were isolated in 85% yield, which were suitable for X-ray diffraction. IR (KBr pellet, cm^{-1}): 3553(b), 3219(b), 2930(w), 2858(w), 1634(m), 1454(m), 1404(m), 1332(m), 1296(w), 1169(s), 1070(s), 1020(m), 939(s), 786(m). Anal. calcd for $C_{12}H_{10}O_7P_2V$: C, 38.1; H, 2.40. Found: C, 38.5; H, 2.53.

Synthesis of $[V_2O_2(H_2O)_2(L3)]\cdot 1.5H_2O$ (3·1.5H_2O). After stirring for 5 min, a solution of NH_4VO_3 (0.100 g, 0.855 mmol), 1,3-phenylenediphosphonic acid (0.101 g, 0.643 mmol), H_2O (10.00 g, 556 mmol), and HF (0.100 mL, 2.90 mmol) at a molar ratio of 1.33:1.00:865:4.51 was heated to 200 °C for 48 h (initial and final pH of 1.5 and 1.5, respectively). Dark blue crystals of **3**·$1.5H_2O$, suitable for X-ray diffraction, were isolated in 20% yield. IR (KBr pellet, cm^{-1}): 3508(w), 3291(b), 1639(m), 1418(m), 1198(s), 1065(s), 1019(m), 939(s), 786(m). Anal. calcd for $C_6H_{11}O_{11.5}P_2V_2$: C, 16.7; H, 2.57. Found: C, 17.0; H, 2.47.

Synthesis of $[V_2O_2(H_2O)_2(L4)]\cdot 2H_2O$ (4·2H_2O). A solution of NH_4VO_3 (0.119 g, 1.017 mmol), 1,2-bis(dimethoxyphosphoryl-)benzene (0.151 g, 0.513 mmol), H_2O (10.00 g, 556 mmol), and HF (0.600 mL, 17.39 mmol) at a molar ratio of 1.98:1.00:1084:33.90 was stirred briefly before heating to 180 °C for 72 h (initial and final pH of 1.0 and 1.5, respectively). Blue rods of **4**·$2H_2O$ were isolated in 80% yield. IR (KBr pellet, cm^{-1}): 3553(b), 3201(b), 2939(w), 2867(w), 1634(m), 1458(m), 1404(m), 1314(m), 1169(s), 1076(s), 1020(m), 944(s), 790(m). Anal. calcd for $C_6H_{12}O_{12}P_2V_2$: C, 16.4; H, 2.75. Found: C, 16.6; H, 2.56.

Synthesis of $[V_2F(OH)(H_2O)_3(L4)]\cdot 2.25H_2O$ (5·2.25H_2O). After stirring briefly, a solution of NH_4VO_3 (0.119 g, 1.017 mmol), 1,2-bis(dimethoxyphosphoryl)benzene (0.154 g, 0.523 mmol), H_2O (10.00 g, 556 mmol), and HF (0.600 mL, 17.39 mmol) at a molar ratio of 1.94:1.00:1063:33.90 was heated to 200 °C for 72 h (initial and final pH of 1.0 and 1.0, respectively). Green rods of **5**·$2.25H_2O$ were isolated in 80% yield. IR (KBr pellet, cm^{-1}): 3445(m), 2939(w), 2849(w), 1553(m), 1539(w), 1503(w), 1454(w), 1183(w), 1106(m), 1083(m), 1029(s), 1007(m), 984(m), 921(w), 700(m). Anal. calcd for $C_{1.5}H_{4.13}F_{0.25}O_{3.06}P_{0.5}V_{0.5}$: C, 15.4; F, 4.07. Found: C, 15.6; F, 4.22.

Synthesis of $[V_3O_3(OH)(H_3L5)_2]\cdot 7.5H_2O$ or $[V_3O_3(OH)\{C_6H_3(C_6H_4PO_3H)_3\}]\cdot 7.5H_2O$ (6·7.5H_2O). A solution of NH_4VO_3 (0.120 g, 1.026 mmol), 1,3,5-tris(phenyl)-4′-triphosphonic acid benzene (0.117 g, 0.214 mmol), H_2O (10.00 g, 556 mmol), and HF (1.000 mL, 28.99 mmol) at a molar ratio of 4.79:1.00:2598:135.5 was stirred briefly before heating to 150 °C for 72 h (initial and final pH of 1.0 and 1.5, respectively). Dark green/black plates of **6**·$7.5H_2O$ were isolated in 25% yield. IR (KBr pellet, cm^{-1}): 3445(s), 2930(m), 2849(m), 1467(m), 1395(w), 1129(s), 1047(s), 980(m), 908(s), 795(m), 722(w). Anal. calcd for $C_{24}H_{26.5}O_{16}P_3V_{1.5}$: C, 38.9; H, 3.61. Found: C, 39.0; H, 3.63.

X-Ray Crystallography. X-ray measurements were performed on a Bruker-AXS SMART-CCD diffactometer at a low temperature (90 K) using graphite-monochromated Mo Kα radiation ($\lambda_{MoK\alpha}$ = 0.71073 Å).[44] The data were corrected for Lorentz and polarization effects and absorption using SADABS.[45] The structures were solved by direct methods. All non-hydrogen atoms were refined anistropically. After all of the non-hydrogen atoms were located, the model was refined against F^2, initially using isotropic and later anisotropic thermal displacement parameters. Hydrogen atoms were introduced in calculated positions and refined isotropically. Neutral atom scattering coefficients and anomalous dispersion corrections were

(42) Ouellette, W.; Yu, M. H.; O'Connor, C. J.; Zubieta, J. *Inorg. Chem.* **2006**, *45*, 7628.
(43) Wang, Z.; Heising, J. M.; Clearfield, A. *J. Am. Chem. Soc.* **2003**, *125*, 10375.
(44) *SMART*, version 5.630; Siemens Analytical X-ray Instruments, Inc., Bruker-AXS: Madison, WI, 1994.
(45) Sheldrick, G. M. *SADABS*; University of Göttingen: Göttingen, Germany, 1996.

Table 1. Summary of Crystallographic Data for the Structures of $[VO(H_2L1)]$ (**1**), $[VO(H_2L2)]$ (**2**), $[V_2O_2(H_2O)_2(L3)]\cdot 1.5H_2O$ (**3**·$1.5H_2O$), $[V_2O_2(H_2O)_2(L4)]\cdot 2H_2O$ (**4**·$2H_2O$), $[V_2F(OH)(H_2O)_3(L4)]\cdot 2.25H_2O$ (**5**·$2.25H_2O$), $[V_3O_3(OH)(H_3L5)_2]\cdot 7.5H_2O$ (**6**·$7.5H_2O$)

	1	**2**	**3**	**4**	**5**	**6**
empirical formula	$C_6H_6O_7P_2V$	$C_{12}H_9O_7P_2V$	$C_6H_{11}O_{11.50}P_2V_2$	$C_6H_{12}O_{12}P_2V_2$	$C_{1.50}H_{4.13}F_{0.25}O_{3.06}P_{0.50}V_{0.50}$	$C_{24}H_{26.5}O_{16}P_3V_{1.5}$
fw	302.99	378.07	430.97	439.98	116.88	740.27
cryst syst	monoclinic	monoclinic	orthorhombic	orthorhombic	orthorhombic	orthorhombic
space group	*P*2(1)/*c*	*P*2(1)/*c*	*P*2(1)2(1)2(1)	*Pca*2(1)	*Pmma*	*Pnma*
a, Å	10.1805(7)	14.5304(18)	7.1733(5)	20.3400(12)	7.0716(7)	14.5749(8)
b, Å	9.3692(7)	9.3432(11)	9.8385(6)	9.0486(5)	10.1515(10)	17.6671(9)
c, Å	10.2303(7)	10.2272(12)	18.2882(12)	7.4146(5)	10.0344(10)	28.9135(15)
α, deg	90	90	90	90	90	90
β, deg	107.727(1)	108.144(2)	90	90	90	90
γ, deg	90	90	90	90	90	90
V, Å^3	929.47(11)	1319.4(3)	1290.68(15)	1364.65(14)	720.34(12)	7445.1(7)
Z	4	4	4	4	8	8
D_{calcd}, g cm^{-3}	2.165	1.903	2.218	2.142	2.174	1.321
μ, mm^{-1}	1.429	1.028	1.757	1.667	1.598	0.574
T, K	90	90	90	90	90	90
λ, Å	0.71073	0.71073	0.71073	0.71073	0.71073	0.71073
R1[a]	0.0296	0.0641	0.0390	0.0313	0.0515	0.0766
wR2[b]	0.0733	0.1371	0.0833	0.0732	0.1280	0.1826

[a] $R1 = \sum|F_o - F_c|/\sum|F_o|$. [b] $wR2 = \{\sum[w(F_o^2 - F_c^2)^2]/\sum[w(F_o^2)^2]^{1/2}\}$; $w = 1/[\sigma^2(F_o^2) + (a\cdot P)^2 + b\cdot P]$; $P = [\mathrm{Max}(F_o^2,0) + 2F_c^2]/3$.

taken from the International Tables, volume C. All calculations were performed using SHELXTL crystallographic software packages.[46,47]

In the case of compound **3**, there is a statistical disorder of the V-terminal oxo-group unit (V2A−O5A and V2B−O5B) above and below the square-pyramidal basal plane defined by O4-O6-O90-O91 (Supporting Information, Figure S3). This behavior is not unusual for V=O_t units in materials of this type.[30] This model refined unexceptionally and was deemed adequate.

Crystallographic details have been summarized in Table 1. Atomic positional parameters, full tables of bond lengths and angles, and anisotropic temperature factors are available in the Supporting Information. The atom-labeling schemes and 50% thermal ellipsoids for **1**−**6** are provided in the Supporting Information, Figures S1−S6, respectively. Selected bond lengths and angles are given in Table 2.

Magnetism. Magnetic susceptibility measurements for **1** and **4** were performed on a 7 T Quantum Design MPMS SQUID magnetometer. Measurements of magnetization as a function of the temperature were performed from 5 to 300 K and in a 5000 G field. The samples were prepared by packing ∼15 mg of them between cotton plugs in a gelatin capsule, cooled in zero applied field, and measured upon warming. Diamagnetic corrections were applied on the basis of Pascal's constants. The data were corrected for the diamagnetism of the sample holder. For compounds **5** and **6**, magnetic data were recorded on 50.6 and 56.2 mg samples, respectively, in the 2−300 K temperature range using a Quantum Design MPMS-XL-7 SQUID spectrometer. Calibrating and operating procedures have been reported previously.[48] The temperature-dependent data were obtained at a magnetic field of $H = 1000$ Oe after zero field cooling.

Results and Discussion

Synthesis and Infrared Spectroscopy. The oxides of this study were prepared by conventional hydrothermal methods.[49−53] These conditions have been amply demonstrated to be effective for solubilizing and crystallizing organic/inorganic materials in general and, more specifically, oxovanadium and oxomolybdenum organophosphonate phases. The reaction mixture consisted of ammonium vanadate, the appropriate arylphosphonate ligand, and HF in water with reaction temperatures in the range 150−200 °C and reaction times of 48 or 72 h. While HF is generally added as a mineralizer to induce solubility and crystal growth, rather than as a constituent of the product, oxyfluorinated products are not unusual for hybrid oxides of vanadium and molybdenum.[42,54,55] In most cases, fluoride incorporation into the product requires relatively high HF/V ratios (3:1 or greater). However, reaction conditions can also influence the product identity. For example, compound **4** $[V_2O_2(H_2O)_2(L4)]\cdot 2H_2O$ was prepared from a solution with a HF/V ratio of 17:1 at 180 °C. Using the same ratio of reactants but raising the temperature to 200 °C provided the oxyfluorinated material $[V_2F(OH)(H_2O)_3(L4)]\cdot 2.25H_2O$ (**5**·$2.25H_2O$). The critical dependence of product composition on hydrothermal reaction parameters has been noted previously. It is also noteworthy that relatively large HF/V ratios were required to induce crystal growth for **1**−**6**, an observation that contrasts with the behavior of the alkyldiphosphonate family where HF/V molar ratios of 0.5:1 or less were employed. In the absence of HF, mixtures of amorphous materials were observed, even upon adjustment of the solution pH. This observation may reflect the solubilizing and crystallization influences of the HF mineralizer.[56−59]

In common with previous examples of the hydrothermal chemistry of vanadium oxides, reduction of the V(V) starting material to V(IV) is observed.[33,42,60,61] Thus, compounds

(46) Sheldrick, G. M. *SHELXTL-Plus*, version 6.14; Bruker-AXS: Madison, WI, 1996.
(47) Sheldrick, G. M. *SAINT-Plus*, version 6.45; Bruker-AXS: Madison, WI, 1996.
(48) O'Connor, C. J. *Prog. Inorg. Chem.* **1979**, *29*, 203.
(49) Whittingham, M. S. *Curr. Opin. Solid State Mater. Sci.* **1996**, *1*, 227.
(50) Laudise, R. A. *Chem. Eng. News* **1987**, *65*, 30.
(51) Lobachev, A. N. *Crystallization Processes Under Hydrothermal Conditions*; Consultants Bureau: New York, 1973.
(52) Gopalakrishnan, J. *Chem. Mater.* **1995**, *7*, 1265.
(53) Zubieta, J. Solid-State Methods, Hydrothermal. In *Comprehensive Coordination Chemistry II*; McCleverty, J. A., Meyer, T. J., Eds.; Elsevier Science: New York, 2004; Vol. *1*, pp 697−709.
(54) Burkholder, E.; Zubieta, J. *Inorg. Chim. Acta* **2004**, *357*, 279.
(55) Burkholder, E.; Golub, V.; O'Connor, C. J.; Zubieta, J. *Inorg. Chem.* **2004**, *43*, 7014.
(56) Kratochvil, J.; Necas, M.; Petricek, V.; Pinkas, J. *Inorg. Chem.* **2006**, *45*, 6562.
(57) Soumahoro, T.; Burkholder, E.; Ouellette, W.; Zubieta, J. *Inorg. Chim. Acta* **2005**, *358*, 606.
(58) Mahenthirarajah, T.; Lightfoot, P. *Chem Commun.* **2008**, 1401.
(59) Mahenthirarajah, T.; Li, Y.; Lightfoot, P. *Inorg. Chem.* **2008**, *47*, 9097.
(60) Bonavia, G.; Haushalter, R. C.; Zubieta, J. *J. Solid State Chem.* **1996**, *126*, 292.

Table 2. Selected Bond Distances (Å) for the Materials of This Study

compound	V−O(F)[a]
$[VO(H_2L1)]$ (**1**)	1.598(1)
	1.973(1)
	1.976(1)
	1.991(2)
	2.000(1)
	2.395(2)
$[VO(H_2L2)]$ (**2**)	1.599(3)
	1.975(3)
	1.975(3)
	1.993(3)
	1.999(3)
	2.390(3)
$[V_2O_2(H_2O)_2(L3)]\cdot 1.5H_2O$ (**3**$\cdot 1.5H_2O$)	
V1	1.619(2)
	1.971(3)
	1.984(2)
	1.990(2)
	1.998(2)
	2.273(2)
V2A	1.591(4)
	1.937(3)
	1.952(3)
	2.006(3), aqua
	2.019(3), aqua
V2B	1.61(4)
	1.864(8)
	1.976(9), aqua
	1.984(8)
	2.088(9), aqua
$[V_2O_2(H_2O)_2(L4)]\cdot 2H_2O$ (**4**$\cdot 2H_2O$)	
V1	1.588(2)
	1.978(2)
	1.991(2)
	2.014(3), aqua
	2.026(3), aqua
V2	1.613(3)
	1.952(2)
	1.968(2)
	1.969(2)
	1.987(2)
$[V_2F(OH)(H_2O)_3(L4)]\cdot 2.25H_2O$ (**8**$\cdot 2.25H_2O$)	
V1	$\begin{cases} 1.918(2), \mathrm{F}\times 2 \\ 1.980(2)\times 4 \end{cases}$
V2	1.906(7), aqua
	1.920(4) × 2
	1.987(5) × 2, aqua
	2.049(7), aqua
$[V_3O_3(H_2O)(H_3L5)_2]\cdot 7.5H_2O$ (**6**$\cdot 7.5H_2O$)	
V1	1.718(4)
	1.981(3) × 2
	1.995(3) × 2
	2.304(5), aqua
V2	1.543(4)
	1.946(4)
	1.960(4)
	1.963(3)
	1.990(3)
	2.553(4)

[a] Esd's in parentheses. Fluoride and aqua ligands are identified.

1−**4** are V(IV) species, and **6** is a mixed valence V(V)/2×V(IV) material. The fluoride-incorporating product **5** exhibits V(III) sites. This is also a common feature of the hydrothermal chemistry of the vanadium oxides, where reduction to V(III) occurs in high fluoride concentrations with concomitant fluoride incorporation.[42,59]

The infrared spectra of **1**−**4** and **6** exhibit a strong band in the 908−944 cm^{-1} range, attributed to the ν(V=O) of the terminal oxo groups. This band does not appear in the spectrum of **5**, which does not possess a terminally bound oxo group. In addition, the spectra are characterized by a series of three or four bands in the 1000−1650 cm^{-1} range, attributed to the phosphonate ligand.

X-Ray Structures. The structures adopted by the compounds of this study reflect the constraints imposed by the substitution mode of the aromatic diphosphonate ligand, that is, whether 1,4, or 1,3, or 1,2. Thus, compounds **1** and **2** exhibit the common structural motif of inorganic V−P−O layers buttressed by the aromatic spacers of the diphosphonate ligands. In contrast, the 1,2 and 1,3 substitution patterns of the diphosphonate ligands in **3** and **4** preclude expansion into three dimensions through layer pillaring, resulting in two-dimensional and unique three-dimensional structures, respectively.

As shown in Figure 1, the structure of $[VO(H_2L1)]$ (**1**) consists of $\{VO(HO_3PR)_2\}$ layers linked through the $\{C_6H_4\}$ groups of the 1,4-phenyldiphosphonate ligand. While the structure is grossly similar to those observed for the aliphatic bridged materials of the $V_xO_y/\{O_3P(CH_2)_nPO_3\}^{4-}$ family of compounds,[27,28,41] several characteristics merit comment. The layer structure of **1** consists of isolated $\{VO_6\}$ octahedra, that is, no V−O−V linkages, with the six coordination geometry defined by a terminal oxo group and five phosphonate oxygen donors, one from each of five phosphorus tetrahedra. This pattern of polyhedral connectivities within the layer is quite distinct from that previously observed for the pillared layer oxovanadates of the type $[V_2O_2(H_2O)\{O_3P\{O_3P(CH_2)_nPO_3\}\}]\cdot xH_2O$ ($n = 2-5$), which exhibit binuclear units of face-sharing $\{VO_6\}$ octahedra and a bridging aqua ligand.[41] Furthermore, while the aliphatic diphosphonate ligands are fully deprotonated, one oxygen of each phosphorus terminus of the 1,4-phenyldiphosphonate is protonated. One of these adopts the common pendant geometry with a P−O distance of 1.567(2) Å, compared to an average distance of 1.508(2) Å for the unprotonated P−O groups. The second P−OH group coordinates to the vanadium, trans to the terminal oxo group. The long V−O distance of 2.395(2) Å reflects both the strong trans influence of the terminal oxo group and protonation of the oxygen donor. The exceptionally long P−O(H) distance of 1.591(2) Å is consistent with protonation in addition to bonding to the vanadium site. While protonated oxygen atoms of phosphate- and phosphonate-containing materials normally adopt a pendant disposition,[25,26,62,63] the crystallographic data seem to support this assignment. The valence sum for O7, the assigned protonation site, is 1.26 in the absence of the proton, while the valence sums for all other phosphonate oxygen atoms bonded to this vanadium site fall in the expected range of 1.91−1.95. The quality of the crystallographic data did not allow direct observation of this hydrogen atom.

While the polyhedral connectivity within the V−P−O layer of **1** is quite distinct from that observed for the aliphatic series $[V_2O_2(H_2O)\{O_3P(CH_2)_nPO_3\}]\cdot xH_2O$ with $n = 2-5$,

(61) Riou, D.; Ferey, G. *J. Solid State Chem.* **1994**, *111*, 422.

(62) Amoros, P.; LeBail, A. *J. Solid State Chem.* **1992**, *97*, 283.

(63) Vaughey, J. T.; Harrison, W. T. A.; Jacobson, A. J. *J. Solid State Chem.* **1994**, *110*, 305.

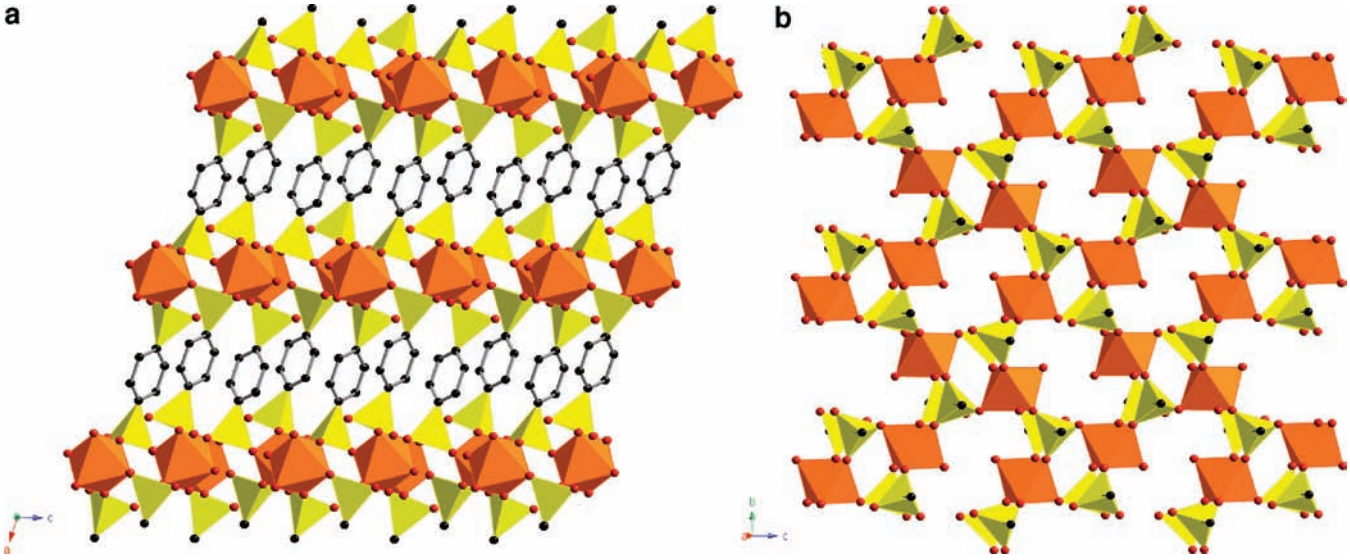

Figure 1. (a) A polyhedral representation of the structure of $[VO(H_2L1)]$ (**1**), viewed normal to the *ac* plane. Color scheme: vanadium, orange polyhedra; phosphorus, yellow polyhedra; oxygen, red spheres; carbon, black spheres. This scheme is used throughout the figures. (b) A view of the V−P−O layer of **1**.

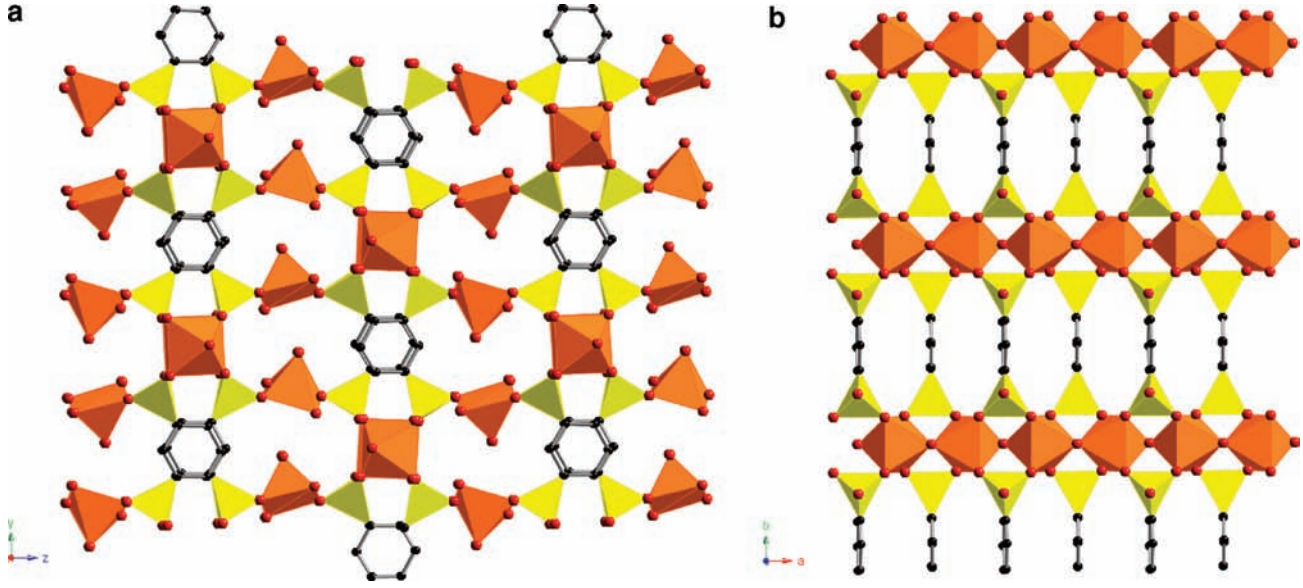

Figure 2. (a) A polyhedral representation of the structure of $[V_2O_2(H_2O)_2(L3)]\cdot 1.5H_2O$ (**3**$\cdot 1.5H_2O$) in the *bc* plane, showing the linking of $\{VO(L3)\}_n^{2n-}$ layers (running parallel to *ab* plane) through the square-pyramidal $\{VO(H_2O)_2O_{2(p)}\}$ units. (b) A view of the $\{VO(L3)\}_n^{2n-}$ layers of **3** in the *ab* plane.

a pattern of isolated $\{VO_6\}$ octahedra and $\{O_3PR\}$ tetrahedra is present for the structures of the type $[V_2O_2(H_2O)\{O_3P(CH_2)_nPO_3\}]\cdot xH_2O$ with $n = 6-8$.[41] The polyhedral pattern of **1** is also somewhat reminiscent of that described for the layers of $Li_2(VO_2)(PO_4)$[64] and β-$VO(HPO_4)\cdot 2H_2O$.[65]

A curious feature of the $V_xO_y/\{O_3P(CH_2)_nPO_3\}^{4-}$ family is the structural dependence on *n*, and consequently the interlamellar spacing. For structures with $n = 2-5$ (type 1), the pillared layer prototype is observed. However, for $n = 6-8$ (type 2), a two-dimensional structure type, $[V_2O_2(H_2O)_4\{O_3P(CH_2)_nPO_3\}]$, consisting of aliphatic tethers sandwiched between V−P−O layers is observed. When $n = 9-12$ (type 3), a third structure type evolves, $[VO\{HO_3P(CH_2)_nPO_3H\}]$, best described as V−P−O double layers tethered through the aliphatic chains (Table 3). The tether distance for compound **1** of 6.370 Å (P to P distance) falls in the range of 4.36−8.30 Å observed for type 1 structures of the $V_xO_y/\{O_3P(CH_2)_nPO_3\}$ series, consistent with the pillared layer structure. However, on the basis of this naı¨ve correlation of structure type and tether length, expansion of the tether length in $[VO(H_2L2)]$ (**2**) might be expected to result in some structural change beyond increasing the interlamellar spacing. While the tether length for **2** of 10.71 Å is more similar to that observed for $[V_2O_2(H_2O)_4\{O_3P(CH_2)_6PO_3\}]$ of 9.50 Å, the layer structure of **2** is identical to that of **1**.

(64) Korthius, V. C.; Hoffmann, R.-D.; Huang, J.; Sleight, A. W. *J. Solid State Chem.* **1993**, *105*, 294.
(65) LeBail, A.; Ferey, G.; Amoros, P.; Beltran-Porter, D.; Villeneuve, G. *J. Solid State Chem.* **1989**, *79*, 169.
(66) LeBail, A.; Ferey, G.; Amoros, P.; Beltran-Porter, D. *Eur. J. Solid State Chem.* **1989**, *26*, 419.

Table 3. Selected Structural Characteristics and Component Building Blocks of Neutral Oxovanadium Organophosphonates

compound	overall dimens.	description	vanadium building blocks	reference
$[VO(H_2O)(O_3PC_6H_5)]$	2-D	V−P−O network	chains of corner-sharing V(IV) octahedral	36
$[(VO)_2(H_2O)_4(O_3PCH_2PO_3)_2]$	2-D	V−P−O network	isolated V(IV) octahedra	67
$[VO(H_2O)(O_3PCH_2NH(C_2H_4)_2\text{-}NHCH_2PO_3)]$	3-D	"pillared" layer	isolated V(IV) octahedra	28
$[(VO)_2(OH)(O_3PCH_2CH_2PO_3)]\cdot H_2O$	3-D	"pillared" layer	binuclear units of face-sharing V(IV)/V(V) $\{VO_5(OH)\}$ octahedra	17
$[V(HO_3PCH_2CH_2PO_3)(H_2O)]$	3-D	V−P−O framework	isolated V(III) octahedra	30
$[(VO)_2(H_2O)\{O_3P(CH_2)_nPO_3\}]\cdot xH_2O$, $n = 2-5$	3-D	"pillared" layer	binuclear units of face-sharing V(IV) octahedra	41
$[(VO)_2(H_2O)_4\{O_3P(CH_2)_6PO_3\}]$	2-D	V−P−O networks sandwiching the alkyl chains	isolated V(IV) octahedra	41
$[(VO)_2(H_2O)\{O_3P(CH_2)_9PO_3)\}]$	3-D	"pillared" V−P−O double layers	binuclear units of corner-sharing V(IV) octahedra	41
$[VO(HO_3P(C_6H_4)_nPO_3H)]$, $n = 1,2$	3-D	"pillared" layers	isolated V(IV) octahedra	this work
$[(VO)_2(H_2O)_2(L3)]\cdot 1.5H_2O$	3-D	V−P−O layers linked through $\{VO_5\}$ square pyramids	chains of corner-sharing $\{VO_6\}$ octahedra and isolated V(IV) square pyramids.	this work
$[(VO)_2(H_2O)_2(L_4)]\cdot 2H_2O$	2-D	V−P−O layers	chains of corner-sharing $\{VO_6\}$ octahedra and isolated V(IV) square pyramids	this work
$[(VO)_3(OH)(H_3L_5)_2]\cdot 7.5H_2O$	2-D	trinuclear $\{V_3O_3(OH)\}$ units linked through $\{C_6H_3(C_6H_4PO_3H)_3\}^{3-}$ units	trinuclear V(IV) clusters	this work

The structural consequences of changing the diphosphonate substitution geometry from 1,4 in compounds **1** and **2** to 1,3 for the compound $[V_2O_2(H_2O)_2(O_3PC_6H_4PO_3)]\cdot 1.5H_2O$ (**3**·1.5H_2O) are illustrated in Figure 2. The complex three-dimensional structure of **3** is constructed from chains of corner-sharing $\{VO_6\}$ octahedra, which are linked through $\{1,3\text{-}O_3PC_6H_4PO_3\}^{4-}$ groups into V−P−O layers which are in turn connected through mononuclear square-pyramidal $\{VO_5\}$ sites to expand the structure in the third dimension.

The chains consist of six coordinate $\{VO_6\}$ sites linked through alternating long−short {V···O═V···} interactions in the axial positions and corner-sharing interactions to four $\{O_3PR\}$ tetrahedra in the equatorial plane. Each diphosphonate ligand links two adjacent chains through two linkages at each chain. The remaining oxygen atom of each $\{O_3PR\}$ terminus bonds to the square-pyramidal $\{VO_5\}$ site.

The square-pyramidal geometry is defined by a terminal oxo group in the apical position, and by trans aqua ligands and trans phosphonate oxygen donors in the basal plane. Each $\{VO_5\}$unit links adjacent $\{VO(O_3PC_6H_4PO_3)\}_n^{2n-}$ layers. The water molecules of crystallization occupy the "interlamellar" cavities between the square-pyramidal vanadium sites.

Structures of the V−P−O family constructed from chains of vanadium polyhedra linked through phosphate or phosphonate polyhedra are not uncommon. Examples include α-$VO(HPO_4)\cdot 2H_2O$,[66] β-$VO(PO_4)$,[67] $VO(H_2PO_4)_2$,[68] $(NH_4)_2$-$(VO)(HPO_4)_2\cdot H_2O$,[69] Cs[$(VO)(HO_3PCH_2PO_3)$],[30] [$(VO)(O_3PPh)$-(H_2O)],[36] and others.[25]

The two-dimensional structure of the 1,2-phenyldiphosphonate derivative $[V_2O_2(H_2O)_2(O_3PC_6H_4PO_3)]\cdot 2H_2O$ (**4**·2H_2O), shown in Figure 3, shows a number of structural motifs similar to those described for **3**. The layer is constructed from chains of corner-sharing $\{VO_6\}$ octahedra linked through 1,2-phenyldiphosphonate groups to mononuclear $\{VO_5\}$ square-pyramidal sites, which in turn serve to link adjacent $\{VO(O_3PC_6H_4PO_3)\}_n^{2n-}$ chains. The $\{VO_6\}_n$ chain of **4** is similar to that of **3**, exhibiting an alternating pattern of long−short {V···O═V···} interactions. However, while the 1,3-phenyldiphosphonate groups of **3** can extend outward from the vanadate chain to connect adjacent chains into a 2-D motif, the 1,2-diphosphonate ligand of **4** is geometrically constrained to fold back and chelate to vanadium sites of a single chain. Two oxygen donors of each $\{O_3PR\}$ terminus are used to bond to the chain, while the remaining oxygen donor of each terminus bonds to a mononuclear $\{VO_5\}$ site.

The square-pyramidal sites exhibit a terminal oxo group and *cis*-aqua ligands and *cis*-oxygen donors from diphos-

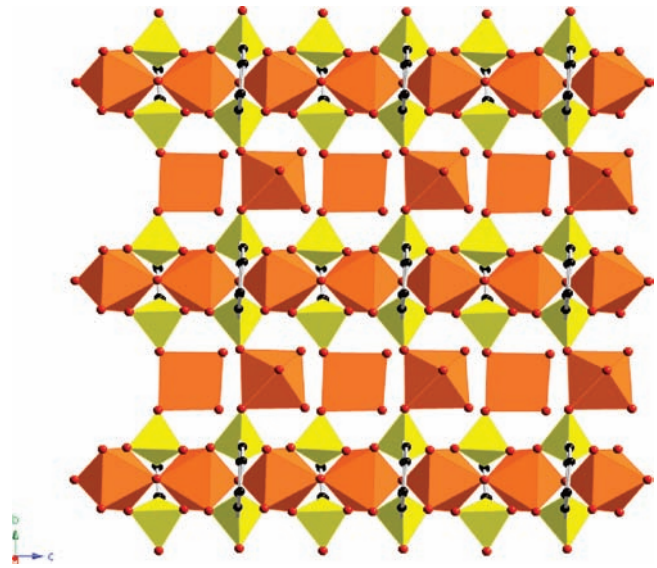

Figure 3. A polyhedral view of the structure of $[V_2O_2(H_2O)_2(L4)]\cdot 2H_2O$ (**4**·2H_2O) in the *bc* plane.

(67) Gopal, R.; Cabeo, C. *J. Solid State Chem.* **1972**, *5*, 432.
(68) Linde, S. A.; Gorbunova, Y. E.; Lavrov, A. V.; Kastnetsov, Y. G. *Dokl. Akad. Nauk SSSR* **1979**, *244*, 1411.
(69) Liu, L.; Wang, X.; Bontchev, R.; Ross, K.; Jacobson, A. J. *J. Mater. Chem.* **1999**, *9*, 1585.

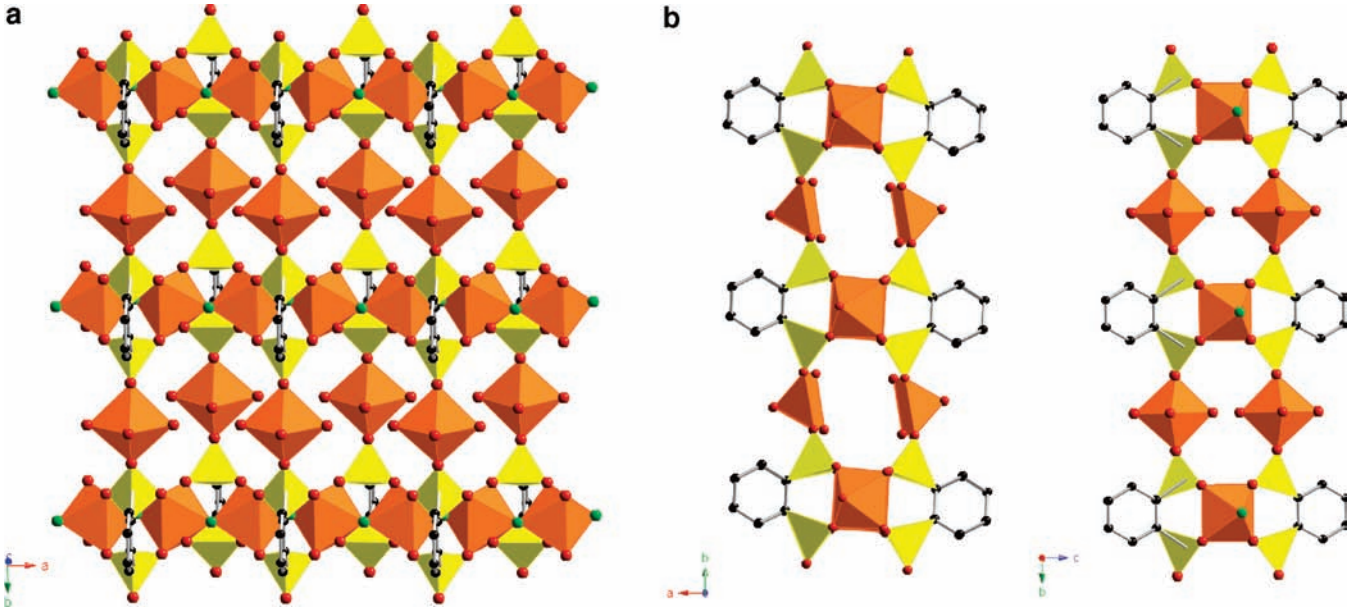

Figure 4. (a) A polyhedral representation of the layer structure of $[V_2F(OH)(H_2O)_3(L4)]\cdot 2.25H_2O$ (**5**·$2.25H_2O$) in the *ab* plane. The fluoride atoms are shown as green spheres. (b) A comparison of the oxovanadium−diphosphonate chain substructures of **4** and **5**.

Table 4. Magnetic Susceptibility Parameters for the Compounds of this Study

compound	fitting model	J (cm^{-1})	zJ' (cm^{-1})	g	Curie constant, C	Weiss constant, θ	μ_{eff} (μ_B) at 300 K
1	Curie-Weiss			2.04	0.424	−3.49	1.84
2	Heisenberg Linear chain	−205	−2.01	1.91			1.68
3	Curie-Weiss			2.06	0.796	0.27	2.50
4	Curie-Weiss			1.97	0.779	0.86	2.51
5	Curie-Weiss			1.94	1.882	0.85	3.77
6	Curie-Weiss			1.95	0.713	−1.66	2.57

phonate ligands of two adjacent chains in the basal plane. One consequence of the connectivity pattern is the generation of eight polyhedra or 16-membered $\{V-O-P-O-\}_4$ rings constructed through the corner-sharing of two octahedral and two square-pyramidal vanadium sites and four phosphonate tetrahedra. The water molecules of crystallization occupy intralamellar sites within these rings, as well as interlamellar sites. The interlamellar spacing is ca. 10.0 Å, although the projection of the phenyl rings and the square-pyramidal sites into this domain severely restricts the free volume.

As shown in Figure 4, the high-temperature, fluoride-incorporating 1,2-phenyldiphosphonate phase, $[V_2F(OH)(H_2O)_3(O_3PC_6H_4PO_3)]\cdot 2.25H_2O$ (**5**·$2.25H_2O$), is also two-dimensional with an overall architecture similar to that of **4**. The structure of **5** may be described as $\{VF(O_3PC_6H_4PO_3)\}_n^{2n-}$ chains, constructed from corner-sharing $\{V(III)F_2O_4\}$ octahedra, decorated with diphosphonate ligands and linked through mononuclear $\{V(III)O_6\}$ subunits into layers in the *ab* plane. Each vanadium site of the chain exhibits trans bridging fluoride ligands, with the remaining four sites occupied by the oxygen donors from four $\{O_3PR\}$ tetrahedra contributed by two 1,2-phenyldiphosphonate groups. Each diphosphonate ligand engages a total of four oxygen donors, two from each $\{O_3PR\}$ terminus, in bonding to the chain. The two remaining phosphonate oxygen donors coordinate to the mononuclear $\{VO_6\}$ sites that serve to bridge the chains. Each of these sites is bonded to *cis*-oxygen donors from the disphosphonate ligands of adjacent chains, three aqua ligands, and a hydroxy group.

In common with the structure of **4**, the fluoride phase **5** consists of vanado−diphosphonate chains linked through mononuclear vanadium polyhedra into a layered architecture. However, while the vanadium chain of **4** consists of $\{V(IV)O_6\}$ octahedra bridged through alternating long−short $\{V\cdots O{=}V\cdots\}$ interactions, the chain of **5** is constructed from $\{V(III)F_2O_4\}$ octahedra bridged through fluoride ligands. Furthermore, the square-pyramidal $\{V(IV)O_5\}$ bridging unit of **4** is replaced by the octahedral $\{V(III)O_6\}$ subunit of **5**. Reduction of the vanadium sites to V(III) is a common feature of fluoride-containing vanadium−diphosphonate structures, although fluoride incorporation is commonly observed in concert with the presence of charge-compensating organoammonium cations. In the syntheses of the fluoride-containing phases, the organoamine component serves not only as a precursor for the cation but as a reducing agent for the vanadium.

The structure of **5** also exhibits a cyclic substructure constructed from the corner-sharing of four V(III) octahedra and four phosphonate tetrahedra, $\{V-O-P-O-\}_4$. An aqua ligand of each $\{V(III)O_6\}$ site projects into the intralamellar cavity generated by these rings. The water molecules of crystallization are encapsulated within these cavities, and curiously, no water is found in the interlamellar regions.

The two-dimensional structure of the aromatic triphosphonate phase, $[V_3O_3(OH)\{C_6H_3(C_6H_4PO_3H)_3\}_2]\cdot 7H_2O$ (**6**·$7H_2O$), is shown in Figure 5. The structure is constructed from trinuclear $\{V_3O_3(OH)(HO_3PR)_6\}$ clusters linked through the idealized C_3-symmetrical 1,3,5-$\{C_6H_3(C_6H_4)_3\}$ backbone

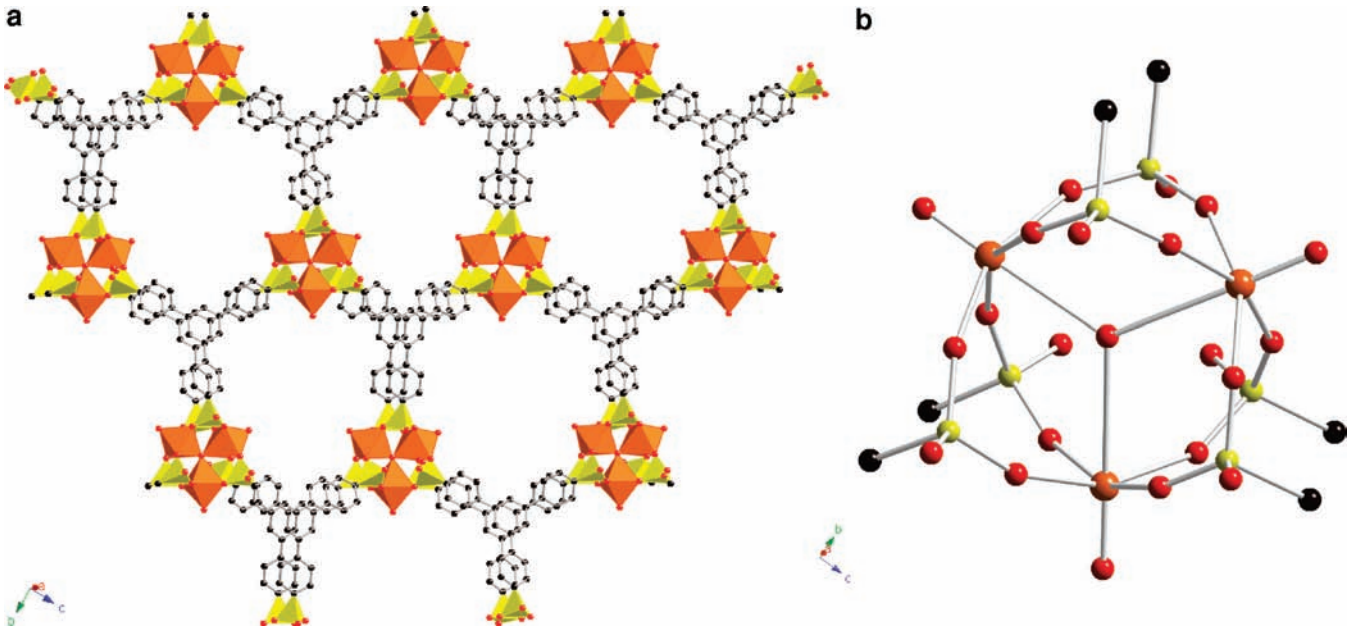

Figure 5. (a) A view of the two-dimensional structure of $[V_3O_3(OH)(H_3L_5)_2]\cdot 7H_2O$ (**6**·$7H_2O$) in the *bc* plane. (b) A ball-and-stick representation of the trinuclear building block of **6**.

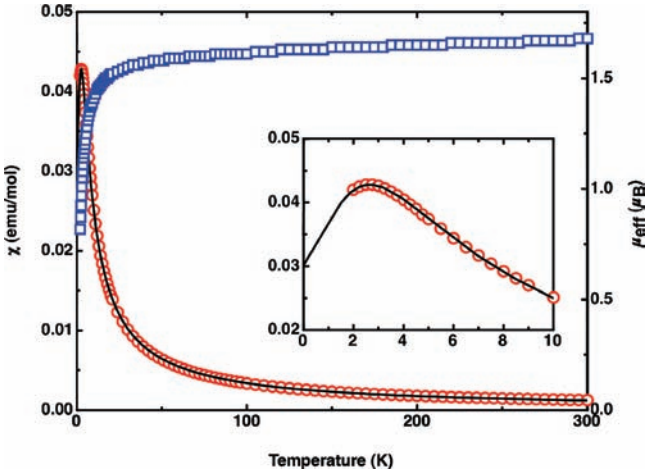

Figure 6. The temperature dependence of χ (red circles) and μ_{eff} (blue circles) of **2** in the 2−300 K range. The inset shows the temperature dependence of $1/\chi$.

of the triphosphonate ligand. The cluster consists of three $\{VO_6\}$ octahedra sharing a common vertex at a μ_3-oxo group. Two vanadium sites have oxo groups trans to this μ_3-oxo group, while the third exhibits a *trans*-hydroxo ligand. The remaining coordination sites are occupied by oxygen donors from six distinct $\{C_6H_3(C_6H_4PO_3H)_3\}^{3-}$ ligands. Each $\{HO_3PR\}^{1-}$ terminus of the triphosphonate ligands bridges two vanadium sites of a cluster. The third oxygen is protonated and pendant. Since each triphosphonate ligand bridges three cluster sites, each cluster is bridged to six adjacent clusters. Pairs of triphosphonate ligands stack in projection in the *bc* plane so as to bridge the same three vanadate clusters, producing a layer that is two-thick in triphosphonate subunits.

The layers are ruffled in profile and stack such that the vanadate clusters of adjacent layers nestle above and below the large cavities of a given layer. The water molecules of crystallization reside in the galleries of approximate dimensions 5.0 × 14.0 Å in the interlamellar domain.

The $\{V_3(\mu_3\text{-}O)\}^{n+}$ has been reported for a number of molecular species. The V(IV) trinuclear complexes $[V_3O_3(THF)(C_6H_5CO_2)_6]$[70] and $[V_3O_3(THF)(CH_3CH_2CO_2)_6]$[71] exhibit the $\{V_3(\mu_3\text{-}O)\}^{10+}$ core with two distinct vanadium coordination spheres. One vanadium site shows a short V-μ_3O distance and a *trans*-THF ligand, while the remaining two vanadium centers establish long V-μ_3O bonds with *trans*-oxo groups. The remaining coordination sites are occupied by oxygen donors from the six bridging bidentate carboxylate ligands. The analogous $\{V_3(\mu_3\text{-}O)\}^{7+}$ core is encountered in the V(III) species $[CH_3CH_2)_3NH][V_3O(Hsalox)(Salax)_2(salmp)]$[72] ($H_2$salox = salicylaldoxime; H_3salmp = 2-(bis(salicylidene-amino)methyl)phenol) and $[V_3O(H_2O)_3(BrCH_2CO_2)_6]$.[73]Compound **6** appears to be the first example of a mixed-valence material with the $\{V_3O\}^{11+}$ core. This assignment is confirmed by the magnetic susceptibility data presented below, as well as by the valence sum calculations[74] for **6** based on the structural determination. The valence sum for the V1 site is 3.94, while that for each of the two V2 sites of the trinuclear unit is 4.50, consistent with a mixed valence and an approximate occupancy of 2×V(IV)/1×V(V).

(70) Cotton, F. A.; Lewis, G. E.; Mott, G. N. *Inorg. Chem.* **1982**, *21*, 3127.
(71) Zhou, W.-B.; Zhang, L.-N.; He, L.-J.; Chen, J.-T.; Zheng, F.-K.; Wa, D.-X.; Huang, X. *Chin. J. Struct. Chem.* **2000**, *19*, 326.
(72) Chaudhuri, P.; Hess, M.; Weyhermuller, T.; Bill, E.; Haupt, H.-J.; Florke, U. *Inorg. Chem. Commun.* **1998**, *1*, 39.
(73) Mukherjee, R.; Ddougan, B. A.; Fry, F. H.; Bunge, S. D.; Ziegler, C. J.; Brasch, N. E. *Inorg. Chem.* **2007**, *46*, 1575.
(74) Brown, I. D. In *Structure and Bonding in Crystals*; O'Keefe, M., Navrotsky, A., Eds.; Academic Press: New York, 1981; Vol. *II*.
(75) Brown, D. A.; Donner, J. A.; Hall, J. W.; Wilson, S. R.; Wilson, R. B.; Hodgson, D. J.; Hatfield, W. E. *Inorg. Chem.* **1979**, *18*, 2635.
(76) Beltran-Porter, D.; Amoros, P.; Ibanez, R.; Martinez, E.; Beltran-Porter, A.; LeBail, A.; Ferey, G.; Villeneuve, G. *Solid State Ionics* **1989**, *32/33*, 57.

Magnetic Properties. Compounds **1**−**6** have been successfully characterized. The results of the fitting of the magnetic susceptibility data for all compounds are summarized in Table 4. Compounds **1**, **3**, and **4** all contain formal V(IV) sites as vanadyl, an $S = 1/2$ ion usually exhibiting essentially complete quenching of orbital angular momentum. The χT versus T data (shown in Supporting Information Figures S13 and S14) are consistent with this picture. After correcting for a small TIP ($\sim 10^{-4}$ emu/mol), the χ^{-1} data for compound **1** can be fit to the Curie−Weiss law, eq 1, resulting in best fit parameters of $g = 2.04$ and $\theta = -3.5$ K for one unpaired electron per formula unit, while compound **3** provided $g = 2.06$, $\theta = 0.27$ K, and $\chi_{TI} = 6.00 \times 10^{-5}$ emu/mol. Similarly, the data from compound **4** can be fit to two $S = 1/2$ sites, giving $g = 1.97$ and $\theta = +1$ K.

$$\chi = \frac{Ng^2\mu_B{}^2Sx(S+1)}{3k(T-\theta)} + \chi_{TI} \quad (1)$$

The behavior of compound **5** is consistent with Curie−Weiss behavior for 2V(III) sites ($S = 1$) with best fit parameters $g = 1.94$, $\theta = +0.85$ K, and $\chi_{TI} = -0.00000723$ emu/mol with $\mu_{eff} = 3.77\mu_B$ at 300 K (calcd. $\mu_{eff} = 4.00\mu_B$) Supporting Information Figure S15).

Compound **2**, which is structurally similar to **1**, exhibits Curie−Weiss behavior in the temperature range 5−300 K. However, below 5 K, a maximum in the χ versus T plot appears at 2.7 K. The magnetic data were found to conform to the simple Heisenberg linear chain model[75] with $S = 1/2$ V^{4+} ions (Figure 6) and were fit to eq 2 by a nonlinear least-squares procedure that weights the data so that the percent difference deviation is minimized.

$$\chi = \chi_0 + \chi_{TI} = \frac{Ng^2\mu_B^2}{kT}\frac{0.25 + 0.14995y + 0.30094y^2}{1.0 + 1.9862y + 0.68854y^2 + 6.0626y^2} + \chi_{TI} \quad (2)$$

where $y = |J|/kT$ and all other parameters have their usual meaning. The calculated susceptibility has also been corrected for exchange interaction zJ' between all spins, as shown in eq 3.

$$\chi' = \frac{\chi_0}{1 - (2zJ'/Ng^2\mu_B^2)\chi_0} \quad (3)$$

The magnetism confirms the mixed-valence character of compound **6** (Figure 7). The best fit to eq 1 with two V(IV) sites gives $g = 1.95$, $\theta = -1.66$ K, and $\chi_{TI} = -0.000392$ emu/mol. The data indicate essentially spin-only magnetism and only very weak intermolecular interactions.

These observations of essentially noninteracting V(IV) sites in **1**, **3**, **4**, and **6** are consistent with previously described magneto-structural correlations for vanadium phosphate phases.[76−78] Significant coupling between V(IV) ions in these structures depends on the proper orientation of the magnetic orbitals with the in-plane oxygen p orbitals. Thus, the polyhedral topology of **1** is similar to that of $VO(HPO_4)\cdot 4H_2O$, which also exhibits poor transmission of magnetic interactions. Similarly, the strongly axially distorted $\{VO_6\}$ octahedra of the vanadyl chain of **4** would not exhibit significant coupling through the μ-oxo bridges due to the mismatch of the magnetic orbitals. A similar argument has been made to explain the magnetic properties of $VO(H_2PO_4)_2$, which is also constructed from $\{VO_6\}_n$ chains. In the case of compound **2**, for which data were collected to 1.9 K rather than to 5 K, a maximum was observed at 2.7 K, consistent with weak antferromagnetic coupling (Table 4).

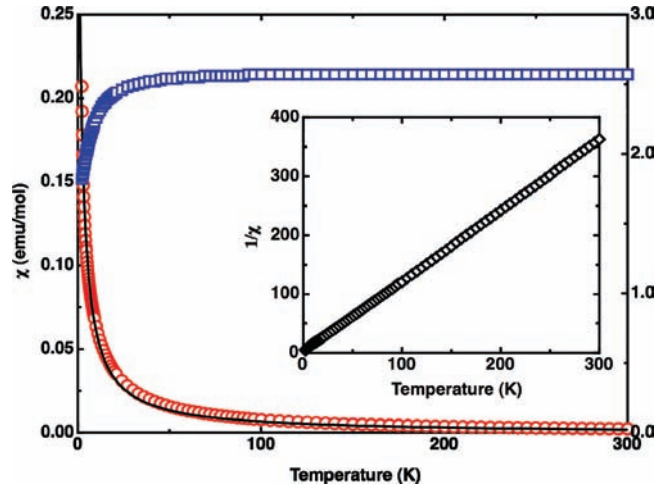

Figure 7. The temperature dependence of χ (red circles) and μ_{eff} (blue circles) of **6** in the 2−300 K range. The inset shows the temperature dependence of $1/\chi$.

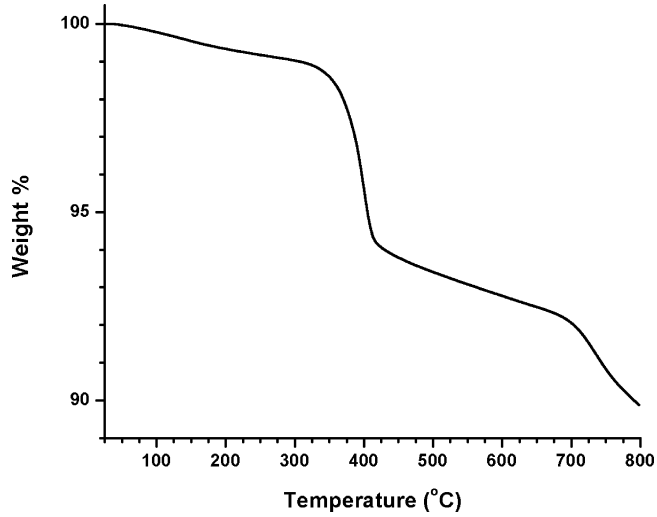

Figure 8. Thermal gravimetric profile for **2** from room temperature to 800 °C.

Thermal Analysis. The TGA profiles of materials **1** and **2** are unexceptional. Compound **1** exhibits no weight loss to ca. 380 °C, whereupon there is a rapid loss of 6% by weight. This initial weight loss is followed by a gradual loss of 4% in the range 440−800 °C. The product of the thermal decomposition is an amorphous powder. As shown in Figure 8, the TGA profile of **2** shows an initial weight loss of 7% at 400 °C, followed by a gradual loss of an additional 2% between 440 and 800 °C. This observation most likely can be attributed to partial decomposition of the organic com-

(77) Roca, M.; Amoros, P.; Cano, J.; Marcos, M. D.; Alamo, J.; Beltran-Porter, A.; Beltran-Porter, D. *Inorg. Chem* **1998**, *37*, 3167.
(78) Huan, G.; Johnson, J. W.; Jacobson, A. J.; Merola, J. S. *J. Solid State Chem.* **1990**, *89*, 220.

ponent, leading to an amorphous oxovanadium phosphate phase. The infrared spectra of heated samples of **2** exhibit no change to ca. 425 °C. Above 425 °C, while the spectra lose some definition, the aromatic peaks between 1650 and 1420 cm^{-1} and at 820 cm^{-1} are still clearly visible (Supporting Information, Figure S11), consistent with only partial loss of the ligand upon heating.

The TGA profile of **3** exhibits a 1.5% weight loss between room temperature and 50 °C, attributed to the loss of water of crystallization (1.54%, theoretical; Supporting Information Figure S19). A second sharp weight loss occurs at 140−220 °C, accounting for 11.5% by weight, followed by a gradual weight loss of an additional 3%. These weight losses may be attributed to the loss of coordinated water and partial decomposition of the hydrocarbon tether.

Compound **4** exhibits a more complex TGA profile, characterized by partial decomposition of the organic component, as well as dehydration. The profile exhibits a total weight loss of 15.5% between room temperature and 220 °C in three steps. These initial weight losses are consistent with the loss of two water molecules of crystallization and two coordinated water molecules (16.4%, theoretical). This is followed by a plateau between 220 and 380 °C, whereupon the organic component starts to slowly decompose. The product of the thermal decomposition is an amorphous gray powder. The thermodiffraction profile of **4** (Supporting Information, Figure S22) confirms that water loss results in loss of crystallinity, as the material is amorphous above 125 °C. However, the infrared spectrum of **4** at 450 °C confirms that the ligand has only partially decomposed, with prominent features attributed to the organophosphonate observed at 1430, 1160, and 780 cm^{-1}.

Compound **5** undergoes a weight loss of ca. 16% between room temperature and 230 °C, followed by a loss of an additional 4% between 230 and 440 °C. This weight loss is consistent with dehydration of the sample, with a loss of both the water of crystallization and the coordinated water (19.3%, theoretical). The thermodiffraction profile of **5** (Supporting Information Figure S25) exhibits a new phase above 150 °C, which persists to 450 °C. The infrared spectrum of a sample of **5** heated to 450 °C retains the features associated with the presence of the organophosphate ligand.

The TGA profile of compound **6** also exhibits dehydration at low temperatures. There is a loss of ca. 11% weight between room temperature and 120 °C, corresponding to the loss of the water of crystallization, as well as the coordinated water. This initial step is followed by a gradual weight loss of 11.5% between 150 and 800 °C. The final product of the thermal process is amorphous. However, the thermal diffraction profiles of **6** indicate that the structure is maintained to 450 °C (Supporting Information, Figure S27).

Conclusions

Hydrothermal reaction conditions have been exploited to prepare six novel materials of the oxovanadium−aryldiphosphonate family. Compounds **1** and **2** exhibit the prototypical buttressed layer architecture, common to many diphosphonate phases. However, the detailed connectivity of the V−P−O layerisquitedistinctfromthoseoftheoxovanadium−alkyldiphosphonate analogues. The consequences of the disposition of the $\{PO_3\}$ groups on the phenyl ring in 1,3- and 1,2-phenyldiphosphonates are manifested in the three-dimensional and two-dimensional structures of **3** and **4**, respectively. The aryltriphosphonate phase **6** exhibits a unique two-dimensional structure, constructed from $\{V_3O\}$ cluster building blocks. Fluoride incorporation provides the unusual two-dimensional phase **5**.

Several vanadium building blocks are embedded in the structures of **1**−**6**, including the above-cited trinuclear unit, isolated square pyramids and octahedra, and chains of corner-sharing $\{VO_6\}$ octahedra. Compounds **3** and **4** exhibit both monoclear $\{VO_5\}$ square pyramids and chains of $\{VO_6\}$ octahedra as component building blocks.

The structural versatility of the oxovanadium−arylphosphonate family (Table 3) reflects the geometric flexibility of the phosponate ligands, as related to the relative disposition of $\{PO_3\}$ groups about the ring and the number of functional groups on the ring. In addition, the interplay of the polyhedral and oxidation state variability of vanadium, the various possibilities for vanadium and phosphorus polyhedral connectivities, variable protonation of $\{PO_3\}$ groups, coordination of aqua ligands, flexibility of P−O(H) bond distances and V−O−P bond angles, and variations of F/V ratios results in an extensive and often unpredictable structural chemistry.

Acknowledgment. This work was supported by a grant from the National Science Foundation, CHE-0604527.

Supporting Information Available: Crystallographic files in CIF format for compounds **1**−**6**. Figures S1−S6 show the atom-labeling schemes and 50% thermal ellipsoid for **1**−**6**. Figures S7−S12 show the observed and calculated powder XRD profiles for **1**−**6**, respectively. Figures S16−27 show the TGA profiles, infrared spectra, and thermodiffraction patterns for compounds **1**−**6**. Figures S13−S15 show the dependences of the magnetic susceptibilityies of **1**, **3**, **4**, and **5** on the temperature. This material is available free of charge via the Internet at http://pubs.acs.org.

IC801450M